Int. J. Appl. Math. Comput. Sci., 2023, Vol. 33, No. 3, 449–461
DOI: 10.34768/amcs-2023-0033

NONSMOOTH OPTIMIZATION CONTROL BASED ON A SANDWICH MODEL WITH HYSTERESIS FOR PIEZO–POSITIONING SYSTEMS

SEN YANG [a], YONGHONG TAN [b,*], RUILI DONG [c], QINGYUAN TAN [d]

[a]College of Mathematics and Physics
Shanghai Normal University
100 Guilin Rd., Shanghai 200234, China
e-mail: 1000423796@smail.shnu.edu.cn

[b]College of Information, Mechanical and Electrical Engineering
Shanghai Normal University
100 Guilin Rd., Shanghai 200234, China
e-mail: tany@shnu.edu.cn

[c]College of Information Science and Technology
Donghua University
2999 North-Renmin Rd., Shanghai 201620, China
e-mail: ruilidong@dhu.edu.cn

[d]R&D Center (PERDC)
Ford Powertrain Engineering
1 Quality Way, Windsor, ON, N9A 6X3, Canada
e-mail: tan.qingyuan@gmail.com

A nonsmooth optimization control (NOC) based on a sandwich model with hysteresis is proposed to control a micropositioning system (MPS) with a piezoelectric actuator (PEA). In this control scheme, the hysteresis phenomenon inherent in the PEA is described by a Duhem submodel embedded between two linear dynamic submodels that describe the behavior of the drive amplifier and the flexible hinge with load, respectively, thus constituting a sandwich model with hysteresis. Based on this model, a nonsmooth predictor for sandwich systems with hysteresis is constructed. To avoid the complicated online search for the optimal value of the generalized gradient at a nonsmooth point, the method of the so-called weighted estimation of generalized gradient is proposed. In order to compensate for the model error caused by model uncertainty, a model error compensator (MEC) is integrated into the online optimization control strategy. Afterwards, the stability of the control system is analyzed based on Lyapunov's theory. Finally, the proposed NOC-MEC method is verified on an MPS with a PEA, and the corresponding experimental results are presented.

Keywords: optimization control, hysteresis, compensation, piezoelectric actuator, sandwich system.

1. Introduction

Many mechatronic systems have sandwich structures wherein nonsmooth nonlinear components such as dead-zone, backlash, or hysteresis are sandwiched in between linear dynamic subblocks, which is also called the Wiener–Hammerstein system with nonsmooth nonlinearities (Luo *et al.*, 2015; Dong *et al.*, 2013; 2016; 2017). A typical sandwich system usually has the structure as shown in Fig. 1, where L_1 is the input linear dynamic subsystem, L_2 is the output linear dynamic subsystem and N represents the nonlinear subsystem, respectively. In precision positioning systems, hysteresis is usually involved in the smart materials-based actuators, such as the actuators made by piezoelectric ceramic, shape memory alloy and electromagnetic materials (Xue *et al.*, 2019; Harnischmacher and Marquardt, 2007; Oliveri

*Corresponding author

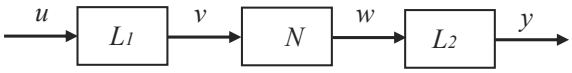

Fig. 1. Sandwich system structure.

et al., 2019; Janaideh *et al*., 2008). A micropositioning stage (MPS) with a piezoelectric actuator (PEA) can be classified as a sandwich system with hysteresis since the piezoelectric actuators in the stage are involved with hysteresis.

Note that hysteresis in the PEA of an MPS is a nonsmooth nonlinearity with a rate-dependent characteristic, which may lead to undesired positioning residuals, phase lag reduction and oscillation, etc., so that the dynamic system performance will be deteriorated. Hence, in order to obtain accurate positioning and satisfactory dynamic performance of MPS, the corresponding controller should have the capability to suppress the influence of the hysteresis.

For the control of the MPS with the PEA, optimization based on a control strategy is one of interesting alternatives. Nowadays, various optimized control strategies of the nonlinear systems have been proposed, e.g., fuzzy control with optimal design (Tong *et al*., 2018), adaptive reconfiguration control (Zhang *et al*., 2022) and adaptive optimizing control (Yu *et al*., 2022; Li *et al*., 2022), etc. These control strategies are applicable for the dynamic systems with monotonic or smooth nonlinear factors. Note that for the dynamic systems with nonlinear factors with nonsmooth and multivalued characteristics such as hysteresis, new optimization control schemes need to be studied.

For the sandwich systems with hysteresis, if the input and output of the embedded hysteresis can be reconstructed, then the inverse model-based control strategy, such as internal model control (Dong *et al*., 2013) and nonlinear decoupling control (Xie *et al*., 2013) are applicable. The advantage of the inverse hysteresis model-based compensation is that the hysteresis effect can be suppressed by the inverse hysteretic model. In addition, it can increase the bandwidth of the system and yield fast system response. However, the obvious disadvantage is that the existence of model uncertainty may degrade the compensation performance. Moreover, building the inverse hysteresis model is not an easy job. In order to avoid building the inverse hysteresis model, Zhao and Tan (2006) proposed a pseudoinverse hysteresis model based adaptive neural network control method.

If the input and output of hysteresis in the sandwich system cannot be reconstructed, then the direct control methods such that sliding mode control strategies (Corradini *et al*., 2005; Manni *et al*., 2008) are applied. On the other hand, Tao *et al*. (2001) proposed a compound control method and Taware *et al*. (2002) developed a hybrid control method for nonsmooth sandwich systems. In addition, Dong *et al*. (2008) proposed a nonsmooth nonlinear programming based predictive control strategy for the systems with backlash-like hysteresis.

It is noted that only the case that the rate-independent hysteresis in the sandwich systems is considered in the aforementioned literature. In fact, in the MPS, the hysteresis inherent in the PEA has a rate-dependent characteristic. Usually, the rate-dependent hysteresis is more complex than the rate-independent case since rate-dependent hysteresis causes the phase lag that varies with input frequency and produces a complicated dynamic phenomenon.

Moreover, in most of the above-mentioned schemes, the online optimization of the control strategy is not considered. However, it is important to consider the online optimization solution for the control strategy to ensure satisfactory control performance. Since the sandwich system with hysteresis is a nonsmooth dynamic system, conventional optimization techniques cannot be directly applied. Therefore, inspired by the above discussion, in this paper, an online optimization control scheme is proposed for the sandwich systems with rate-dependent hysteresis.

Due to the nonsmooth feature of hysteresis, the optimization control for sandwich system with hysteresis will face the challenge that the gradients will not exist at nonsmooth points. Therefore, the subgradients should be introduced to deal with this problem. Usually, the computation of subgradients calls for an offline method (Clarke *et al*., 1998). However, the real-time control strategy needs to consider the online scheme of nonsmooth optimization, so it is necessary to study the online optimization control strategy based on the subgradient technique. Note that subgradients at nonsmooth points tend to have multiple values; therefore subgradients can be represented as closed intervals at nonsmooth points, which may lead to complex search computations. If subgradient-based online optimization is implemented, then it may become a computational burden for real-time control. To simplify computations, a novel method is proposed to approximate the subgradients at nonsmooth points using smooth interpolation-based estimates.

Subsequently, for reducing the effect of model uncertainty to system performance, a model error compensator (MEC) is introduced to the nonsmooth d-step-ahead predictor based on the sandwich model with rate-dependent hysteresis. Then, a nonsmooth optimization control (NOC) scheme with MEC is proposed for online optimized tuning of the control mechanism towards the minimization of the control

cost function. By introducing the MEC, the proposed nonsmooth optimization control with a model error compensator (NOC-MEC) scheme has the following advantages:

(i) Considering robust control usually requires conservative design by sacrificing the transient performance of the system. The proposed NOC-MEC method can improve the prediction accuracy of the system by introducing the MEC. Then, the corresponding NOC-MEC strategy does not need to be conservatively designed to tolerate model uncertainty.

(ii) Noting that the adaptive control scheme requires online estimation of model parameters, updating the parameters of a sandwich model with rate-dependent hysteresis online is not an easy task. This is time-consuming and results in a large computational cost. The proposed NOC-MEC strategy does not need to update the parameters of the system model online and is therefore computationally simpler than the adaptive control method.

Therefore, the main contributions of this paper are as follows:

(i) A subgradient based nonsmooth optimization control scheme is proposed to deal with the control of micropositioning systems with rate-dependent hysteresis.

(ii) A method of interpolation-based estimation is proposed to approximate the subgradients at nonsmooth points, which simplifies the search process of sub-gradients.

(iii) A model error compensator is integrated in the control scheme to suppress the effect of unknown model mismatches.

The organization of this paper is as follows. In Section 2, the sandwich model with hysteresis used to describe the MPS with the PEA is briefly described. Then, based on the sandwich model with hysteresis, the NOC-MEC is constructed in Section 3. In Section 4, the stability analysis of the control system is presented. Afterward, in Section 5, the proposed NOC-MEC method is verified on the displacement control of an MPS with a PEA. Finally, conclusions of the paper are presented in Section 6.

2. Sandwich model with hysteresis

In the sandwich model with hysteresis used to describe the behavior of the micropositioning stage, the linear dynamic subsystems L_1 and L_2 are used to describe the properties of the driving circuit and the flexible hinge with load, which can be respectively depicted by

$$L_1 : A_1(q^{-1})v(k) = q^{-d}B_1(q^{-1})u(k) \tag{1}$$

and

$$L_2 : A_2(q^{-1})y(k) = B_2(q^{-1})w(k), \tag{2}$$

where $u(k) \in \mathbb{R}$ and $y(k) \in \mathbb{R}$ represent the input voltage of the MPS and output displacement of the MPS, respectively, while $v(k) \in \mathbb{R}$ and $w(k) \in \mathbb{R}$ are internal variables of the system and cannot be measured directly. Here q^{-1} is the unit back-shift operator (i.e., $q^{-1}x(k) = x(k-1)$), as well as $A_1(q^{-1}), B_1(q^{-1}), A_2(q^{-1})$ and $B_2(q^{-1})$ are polynomials which can be expressed as

$$\begin{aligned}
A_1(q^{-1}) &= 1 + a_{11}q^{-1} + \cdots + a_{1n_{1a}}q^{-n_{1a}},\\
B_1(q^{-1}) &= b_{10} + b_{11}q^{-1} + \cdots + b_{1n_{1b}}q^{-n_{1b}}, \quad b_{10} \neq 0,\\
A_2(q^{-1}) &= 1 + a_{21}q^{-1} + \cdots + a_{2n_{2a}}q^{-n_{2a}},\\
B_2(q^{-1}) &= b_{20} + b_{21}q^{-1} + \cdots + b_{2n_{2b}}q^{-n_{2b}}, \quad b_{20} \neq 0,
\end{aligned}$$

respectively, where n_{1a}, n_{1b}, n_{2a} and n_{2b} are the orders of the polynomials $A_1(q^{-1}), B_1(q^{-1}), A_2(q^{-1})$ and $B_2(q^{-1})$, respectively; d denotes the time delay, and $a_{11}, \ldots, a_{1n_{1a}}, b_{10}, \ldots, b_{1n_{1b}}, a_{21}, \ldots, a_{2n_{2a}}$ and $b_{20}, \ldots, b_{2n_{2b}}$ as well as d are known coefficients.

On the other hand, to describe the characteristic of rate-dependent hysteresis in the piezoelectric actuator of the MPS, the Duhem model (Oh and Bernstein, 2005; Dong *et al.*, 2016; 2017) is employed, i.e.,

$$\begin{aligned}
N : w(k) = w(k-1) &+ \alpha[f_0 \operatorname{sgn}(v(k-1))\\
&+ f_1 v(k-1) - w(k-1)]|\Delta v(k)|\\
&+ g_0 \Delta v(k),
\end{aligned} \tag{3}$$

where $\operatorname{sgn}(x)$ is the sign function, α, f_0, f_1 and g_0 are known coefficients satisfying the dissipative condition, i.e., $g_0 > 0$ and $g_0 \leq f_1$, as well as the stability condition: $0 < \alpha|\Delta v(k)| < 2$, where $\Delta v(k) = v(k) - v(k-1)$ (Dong *et al.*, 2017).

Hence, the corresponding sandwich model with rate-dependent hysteresis can be described by (1), (2) and (3).

The goal of this paper is to design the NOC-MEC scheme for the micropositioning stage with a piezoelectric actuator, which has a sandwich structure with rate-dependent hysteresis, such that the cost function is minimized and the system output can track the reference trajectory of the system.

3. NOC-MEC strategy

In this section, the NOC-MEC strategy is developed based on the prediction of the sandwich system with rate-dependent hysteresis. The architecture of the system

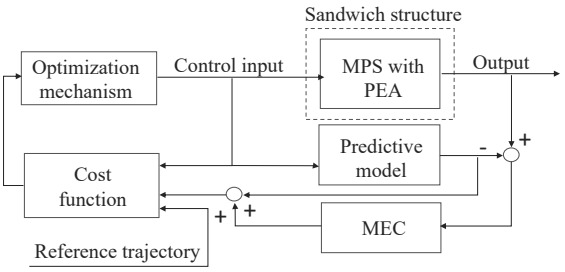

Fig. 2. Architecture of the proposed NOC-MEC method.

with NOC-MEC scheme is shown in Fig. 2. In this architecture, the reference trajectory, the outputs of the controller, the MPS with the PEA model and the MEC are fed to form the cost function. Then, the cost function is minimized online by the optimization mechanism to generate the corresponding optimization control.

3.1. Prediction based on the nonsmooth sandwich model. Because v and w are usually not measured directly, they need to be estimated based on submodels $L_1(\cdot)$ and $N(\cdot)$. Therefore, by using the Diophantine equation (Clarke *et al*., 1987), i.e.,

$$1 = Q(q^{-1})A_1(q^{-1}) + q^{-d}H(q^{-1}), \tag{4}$$

where

$$\begin{aligned} Q(q^{-1}) &= 1 + q_1 q^{-1} + \cdots + q_{d-1}q^{-(d-1)}, \\ H(q^{-1}) &= h_0 + h_1 q^{-1} + \cdots + h_{n_{1a}-1}q^{-(n_{1a}-1)} \end{aligned}$$

and the coefficients of polynomials $Q(q^{-1})$ and $H(q^{-1})$ are described by

$$q_i = -\sum_{s=1}^{i} q_{i-s}a_{1s}, \quad i = 1, 2, \ldots, d-1,$$

$$h_j = -\sum_{s=0}^{d-1} q_{d-1-s}a_{1,j+s+1}, \quad j = 0, 1, \ldots, n_{1a}-1,$$

respectively, the corresponding d-step-ahead predictor is derived by

$$\hat{v}(k+d|k) = H(q^{-1})v(k) + R(q^{-1})u(k), \tag{5}$$

where

$$\begin{aligned} R(q^{-1}) &= Q(q^{-1})B_1(q^{-1}) \\ &= r_0 + r_1 q^{-1} + \cdots + r_{n_{1b}+d-1}q^{-(n_{1b}+d-1)}, \end{aligned}$$

$$r_i = \sum_{j=0}^{i} b_{1,i-j}q_j, \quad i = 0, 1, \ldots, n_{1b}+d-1.$$

By substituting (5) into (3), the prediction of the hysteresis in between $L_1(\cdot)$ and $N(\cdot)$ will be

$$\begin{aligned} N : \hat{w}(k+d|k) &= \hat{w}(k+d-1)) \\ &+ \alpha[f_0 \operatorname{sgn}(\hat{v}(k+d-1) + f_1\hat{v}(k+d-1) \\ &- \hat{w}(k+d-1)]|\Delta\hat{v}(k+d|k)| \\ &+ g_0\Delta\hat{v}(k+d|k), \end{aligned} \tag{6}$$

Then, by combining (6) and (2), the prediction of the sandwich system with hysteresis is obtained, i.e.,

$$\begin{aligned} \hat{y}(k+d|k) =& A_{21}(q^{-1})\hat{y}(k+d-1) \\ &+ B_2(q^{-1})\hat{w}(k+d|k), \end{aligned} \tag{7}$$

where $A_{21}(q^{-1}) = -a_{21}q^{-1} - \cdots - a_{2n_{2a}}q^{-(n_{2a}-1)}$.

Thus, (5)–(7) represent the d-step-ahead nonsmooth predictor of the sandwich system with hysteresis.

3.2. NOC-MEC strategy. Usually, the model uncertainty caused by modeling residuals cannot be ignored. To compensate the impact of model uncertainty on the control system performance, an MEC is introduced to improve the accuracy of the system prediction, i.e.,

$$\begin{aligned} \bar{y}(k+d) &= \hat{y}(k+d|k) + \phi(\varepsilon(k)) \\ &= A_{21}(q^{-1})\hat{y}(k+d-1) \\ &\quad + B_2(q^{-1})\hat{w}(k+d|k) + \phi(\varepsilon(k)), \end{aligned} \tag{8}$$

where $\varepsilon(k) = y(k) - \hat{y}(k)$ and

$$\phi(\varepsilon(k)) = \sigma[y(k) - \hat{y}(k)] \tag{9}$$

is the MEC, where $\sigma > 0$ is the compensation factor.

Define the cost function of the control system as

$$J = \frac{1}{2}[e(k+d)]^2 + \frac{\lambda}{2}[\Delta u(k)]^2, \tag{10}$$

where $\lambda > 0$ is the weighting factor and

$$\begin{aligned} e(k+d) &= r_s(k+d) - \bar{y}(k+d) \\ &= r_s(k+d) - \hat{y}(k+d|k) - \phi(\varepsilon(k)) \end{aligned} \tag{11}$$

is the prediction error, where r_s denotes the reference trajectory.

Assumption 1. Assume that the cost function (10) has at least one extremum.

Letting $0 \in \partial_{u(k-1)}J[u(k-1)]$ leads to

$$u(k) = u(k-1) + \gamma e(k+d)\partial_{u(k-1)}e(k+d), \tag{12}$$

where $\gamma = 1/\lambda$ is optimizing stepsize and the subgradient of $e(k+d)$ with respect to $u(k-1)$ is

$$\begin{aligned}\partial_{u(k-1)} e(k+d) = &-\partial_{u(k-1)}\hat{y}(k+d|k) \\ &- \partial_{u(k-1)}\phi(\varepsilon(k)),\end{aligned} \tag{13}$$

where

$$\begin{aligned}\partial_{u(k-1)}\hat{y}(k+d|k) =&\partial_{\hat{w}(k+d|k)}\hat{y}(k+d|k)\cdot(\partial_{\hat{v}}\hat{w})_k \\ &\cdot \partial_{u(k-1)}\hat{v}(k+d|k),\end{aligned} \tag{14}$$

with $(\partial_{\hat{v}}\hat{w})_k = \partial_{\hat{v}(k+d|k)}\hat{w}(k+d|k)$. Based on (7),

$$\partial_{\hat{w}(k+d|k)}\hat{y}(k+d|k) = b_{20}, \tag{15}$$

and in terms of (5),

$$\partial_{u(k-1)}\hat{v}(k+d|k) = r_1. \tag{16}$$

Moreover, for the convenience of analysis, let

$$\begin{aligned}F_k^+ =&g_0 + \alpha[f_0\,\mathrm{sgn}(\hat{v}(k+d-1)) \\ &+ f_1\hat{v}(k+d-1) - \hat{w}(k+d-1)]\end{aligned} \tag{17}$$

and

$$\begin{aligned}F_k^- =&g_0 - \alpha[f_0\,\mathrm{sgn}(\hat{v}(k+d-1)) \\ &+ f_1\hat{v}(k+d-1) - \hat{w}(k+d-1)].\end{aligned} \tag{18}$$

Based on (6), $(\partial_{\hat{v}}\hat{w})_k$ in the smooth segments of rate-dependent hysteresis is

$$(\partial_{\hat{v}}\hat{w})_k = \begin{cases} F_k^+, & \Delta\hat{v}(k+d|k) > 0, \\ F_k^-, & \Delta\hat{v}(k+d|k) < 0. \end{cases}$$

However, at the nonsmooth points of rate-dependent hysteresis, the gradient does not exist. In this case, $\hat{w}$ is not differentiable. Hence, the corresponding subgradient is introduced. At a nonsmooth point, $\hat{w}$ has many subgradients. Figure 3 illustrates the subgradients of hysteresis at the nonsmooth point A: only two subgradients, s_1 and s_2, where $s_1 = (\partial_{\hat{v}_1}\hat{w})_{k-i}$ and $s_2 = (\partial_{\hat{v}_2}\hat{w})_{k-i-1}$, are shown. Thus, it can be expressed as a closed interval at nonsmooth points (Clarke *et al.*, 1998), i.e., $(\partial_{\hat{v}}\hat{w})_k = [F_k^-, F_k^+]$.

Since determination of the subgradient at a nonsmooth point entails the search for all possible gradient values in a closed interval, and then selection of an optimal one, the computational burden of the online optimization search may be quite high.

To simplify the online search for the subgradient at a nonsmooth point, an approximation of the subgradient via smooth function-based estimation is proposed.

Lemma 1. (Chen, 2012) *Suppose* $\hat{w}(k+d|k) = D[\hat{v}(k+d|k)]$ *is locally Lipschitz continuous and* $G[\hat{v}(k+d|k), \beta]$

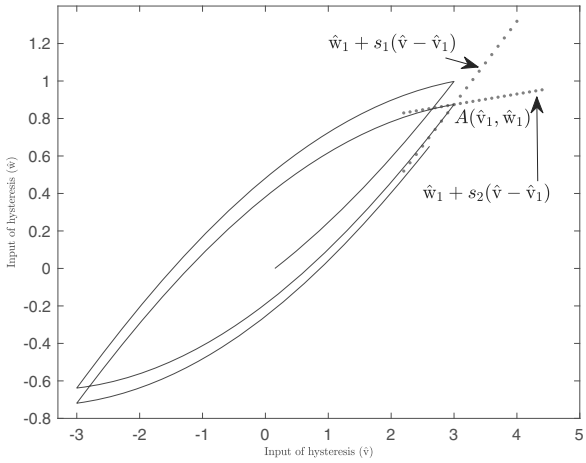

Fig. 3. Multiple values of the subgradient at nonsmooth points.

is a smoothing function of $D(\cdot)$ *for any fixed* $\beta > 0$. *Then, for any* $\hat{v}$,

$$\left\{ \lim_{\hat{v}^k \to v, \beta_k \downarrow 0} \nabla_v \tilde{D}(\hat{v}^k, \beta_k) \right\}$$

is nonempty, bounded and $\partial D(\hat{v}) = G_{\tilde{D}}(\hat{v})$,*where the Clarke subdifferential* $\partial D(\hat{v}) = \mathrm{con}\{\hat{v} | \nabla D(z) \to \hat{v}, D$ *is differentiable at* $z, z \to \hat{v}\}$ *and the subdifferential associated with the smoothing function* $G_{\tilde{D}}(\hat{v}) = \mathrm{con}\{\hat{v} | \nabla_{\hat{v}}\tilde{D}(\hat{v}^k, \beta_k) \to \hat{v}$, *for* $\hat{v}^k \to \hat{v}, \beta_k \downarrow 0\}$, *where* con *denotes the convex hull of a set.*

Based on Lemma 1, interpolation between the left and right gradients of $\hat{w}(k+d|k)$ with respect to $\hat{v}(k+d|k)$ approaching the extremum points is applied, i.e., $(\partial_{\hat{v}}\hat{w})_k = \beta_k F_k^+ + (1-\beta_k)F_k^-$, where $0 < \beta_k < 1$. According to the above analysis, $(\partial_{\hat{v}}\hat{w})_k$ is approximated by

$$\begin{aligned}&(\partial_{\hat{v}}\hat{w})_k \\ &= \begin{cases} F_k^+, & \Delta\hat{v}(k+d|k) > 0, \\ \beta_k F_k^+ + (1-\beta_k)F_k^-, & \Delta\hat{v}(k+d|k) = 0, \\ F_k^-, & \Delta\hat{v}(k+d|k) < 0. \end{cases}\end{aligned} \tag{19}$$

Remark 1. In (19),

$$\beta_k = \frac{1}{1 + \exp(-m(\partial_{\hat{v}}\hat{w})_{k-1})},$$

where $m > 0$ determines the slope of the exponential function. Obviously, β_k varies with $(\partial_{\hat{v}}\hat{w})_{k-1}$. If $(\partial_{\hat{v}}\hat{w})_{k-1} \geq 0$, $0.5 \leq \beta_k < 1$, in this case F_k^+ will dominate the interpolation. On the other hand, when $(\partial_{\hat{v}}\hat{w})_{k-1} < 0$, it results in $0 \leq \beta_k < 0.5$. Therefore, F_k^- plays a major role in this case.

Then, substituting (15) and (16) into (14) yields

$$\partial_{u(k-1)}\hat{y}(k+d|k) = r_1 b_{20}(\partial_{\hat{v}}\hat{w})_k. \tag{20}$$

Defining $\psi(k) = \partial_{u(k-1)} e(k+d)$ and combining (13) and (20) leads to

$$\psi(k) = r_1 b_{20} (\partial_{\hat{v}} \hat{w})_k - \partial_{u(k-1)} \phi(\varepsilon(k)), \quad (21)$$

where the subgradient $\partial_{u(k-1)}\phi(\varepsilon(k))$ is approximated by the finite difference, i.e., $\partial_{u(k-1)}\phi(\varepsilon(k)) \approx [\phi(\varepsilon(k, u(k-1) + \tau)) - \varepsilon(k, u(k-1) - \tau))]/(2\tau), \tau > 0$; here τ is a very small positive number. Based on (12), the corresponding NOC-MEC scheme for the sandwich system with hysteresis described by (1)–(3) becomes

$$u(k) = u(k-1) + \gamma e(k+d)\psi(k). \quad (22)$$

From the above analysis, it can be seen that the NOC-MEC method not only considers the suppression of hysteresis effect, but also compensates the influence of model uncertainty.

Remark 2. In order to obtain the control strategy (22), the generalized-gradient of the nonsmooth cost function with respect to control input is applied. Similarly to hysteresis phenomenon, dead-zone and backlash also have nonsmooth nonlinear characteristics; therefore, the proposed method can also be used for the control of sandwich systems with dead-zone or backlash.

4. Stability analysis

In this section, the stability of the sandwich systems with hysteresis using NOC-MEC scheme will be analyzed.

Lemma 2. *If $L_1(\cdot) < +\infty$, $L_2(\cdot) < +\infty$ and Eqn. (3) satisfies $0 < \alpha|w(k) - w(k-1)| < 2$ (Dong et al., 2017), the sandwich system with hysteresis described by (1)–(3) is a stable system with bounded input and bounded output (BIBO).*

Proof. Please refer to Appendix A. ■

To investigate the properties of subgradient $\psi(k)$ represented by (21), we use the following result.

Lemma 3. *If $u(k)$ is bounded and $|\partial_{u(k-1)}\phi(\varepsilon(k))| \leq \eta_0$, where η_0 is an upper bound, then there exists $\eta_v > 0$ such that $|\psi(k)| \leq \eta_v$, where $\psi(k)$ is described by (21).*

Proof. Please refer to Appendix B. ■

Then, the stability condition can be derived based on the following result.

Theorem 1. *Assume that the NOC-MEC strategy (21) and (22) is applied to the system described by (1)–(3). Suppose that the factor is chosen as $\rho = \rho_0 + 2\psi^2(k)$, where $\rho_0 > 0$ is a constant and $\psi(k)$ is described by (21). If the optimizing stepsize γ satisfies*

$$0 < \gamma \leq \frac{2}{\rho_0 + \psi^2(k)}, \quad (23)$$

then the control system is stable and $e(k+d, u(k)) \to e^*$ as $k \to \infty$, where $e^* = \min_k\{|e(k+d, u(k))|\} \to 0$.

Proof. Define Lyapunov's function of the system as

$$V(k) = e^2(k+d, u(k)) + \rho[\Delta u(k)]^2. \quad (24)$$

Rearranging (22) leads to

$$\Delta u(k) = \gamma\psi(k)e(k+d, u(k)). \quad (25)$$

Then

$$\begin{aligned} e(k+d, u(k)) &= e(k+d, u(k-1)) \\ &\quad + \Delta e(k+d, u(k)), \end{aligned} \quad (26)$$

where

$$\begin{aligned} \Delta e(k+d, u(k)) &\approx \frac{\partial e(k+d, u(k)}{\partial u(k)} \Delta u(k) \\ &= -\psi(k)\Delta u(k). \end{aligned} \quad (27)$$

Thus, combining (25) and (27) results in

$$\Delta e(k+d, u(k)) = -\gamma\psi^2(k)e(k+d, u(k)). \quad (28)$$

Based on (25), (26) and (28), this yields

$$\begin{aligned} &e^2(k+d, u(k)) - e^2(k+d, u(k-1)) \\ &\quad = \gamma\psi^2(k)[\gamma\psi^2(k)e^2(k+d, u(k)) \\ &\qquad - 2e(k+d, u(k-1))e(k+d, u(k)]. \end{aligned} \quad (29)$$

Substituting (28) into (26) leads to

$$e(k+d, u(k-1)) = (1 + \gamma\psi^2(k))e(k+d, u(k)). \quad (30)$$

From (29) and (30), this implies

$$\begin{aligned} &e^2(k+d, u(k)) - e^2(k+d, u(k-1)) \\ &\quad = -\gamma\psi^2(k)(2 + \gamma\psi^2(k))e^2(k+d, u(k)). \end{aligned} \quad (31)$$

Furthermore, based on (25) and (31), this results in

$$\begin{aligned} &e^2(k+d, u(k)) - e^2(k+d, u(k-1)) + \rho[\Delta u(k)]^2 \\ &\quad = \gamma\psi^2(k)e^2(k+d, u(k))[(\rho - \psi^2(k))\gamma - 2]. \end{aligned} \quad (32)$$

According to (24) and (32), we have

$$\begin{aligned} &V(k) - V(k-1) \\ &\quad = e^2(k+d, u(k)) + \rho[\Delta u(k)]^2 \\ &\qquad - e^2(k+d, u(k-1)) - \rho[\Delta u(k-1)]^2 \\ &\quad \leq \gamma\psi^2(k)e^2(k+d, u(k))[(\rho - \psi^2(k))\gamma - 2]. \end{aligned} \quad (33)$$

If γ is chosen such that

$$0 < \gamma \leq \frac{2}{\rho_0 + \psi^2(k)},$$

where $\rho = \rho_0 + 2\psi^2(k)$, $\rho_0 > 0$, we get $V(k) - V(k-1) \leq 0$. Thus, we have $V(k) \leq V(k-1) \leq \cdots \leq V(0)$; in other words, $\{V(k)\}$ is a monotonically

decreasing sequence. Thereby, $\{V(k)\}$ converges to a nonnegative scalar $V^* > 0$ such that $\lim_{k\to+\infty} V(k) = V^*$. Therefore, the control system is stable.

For $e^* = \min_k\{|e(k+d,u(k))|\}$, we have

$$\begin{cases} 1 - \frac{e^*}{e(k+d,u(k))} = 0, & e(k+d,u(k)) = e^*, \\ 0 < 1 - \frac{e^*}{e(k+d,u(k))} \le 2, & \text{otherwise.} \end{cases} \tag{34}$$

Subtracting e^* from both the sides of (26) and considering (28) yields

$$\tilde{e}(k) = \tilde{e}(k-1) - \gamma\psi^2(k)e(k+d,u(k)). \tag{35}$$

where $\tilde{e}(k) = e(k+d,u(k)) - e^*$. Hence

$$\begin{aligned} \tilde{e}^2(k) &= \tilde{e}^2(k-1) - 2\gamma\psi^2(k)e^2(k+d,u(k)) \\ &\quad \times \left[1 - \frac{e^*}{e(k+d,u(k))}\right] \\ &\quad - \gamma^2\psi^4(k)e^2(k+d,u(k)) \\ &\le \tilde{e}^2(k-1). \end{aligned}$$

Thus, $\{\tilde{e}^2(k)\}$ is a monotonically decreasing sequence. Thereby, $\{\tilde{e}^2(k)\}$ converges to its minimum $(\tilde{e}_k^*)^2$ as k goes to infinity, that is, $\lim_{k\to+\infty} \tilde{e}^2(k) = (\tilde{e}_k^*)^2$.

Moreover, from (34) and (35) it follows that

$$\frac{\tilde{e}^2(k)}{\tilde{e}^2(k-1)} = \left(1 + \frac{\gamma\psi^2(k)}{1 - \frac{e^*}{e(k+d,u(k))}}\right)^{-2}. \tag{36}$$

Denote by σ_k the right-hand side of (36).

If $e^* \neq e(k+d,u(k))$, then $\sigma_k \in (0,1)$. Let $\sigma = \max_k\{\sigma_k\} \in (0,1)$. Therefore,

$$0 \le \tilde{e}^2(k) \le \sigma\tilde{e}^2(k-1) \le \cdots \le \sigma^k\tilde{e}^2(0), \tag{37}$$

where $\tilde{e}^2(0)$ is a constant. Thus, $\lim_{k\to+\infty} \tilde{e}^2(k) = 0$ and $\lim_{k\to+\infty} e(k+d,u(k)) = e^*$.

If $e^* = e(k+d,u(k))$, this yields $\tilde{e}^2(k) = \tilde{e}^2(k-1)$. Based on Assumption 1, it is known that $\tilde{e}^2(k)$ arrives at an extremum, i.e., $\lim_{k\to+\infty} e(k+d,u(k)) = e^*$. ■

Theorem 2. *If the control strategy (22) is applied to the system described by (1)–(3), the system output can track the reference trajectory accurately in steady state, i.e., $e(k+d) \to 0$, as $k \to \infty$.*

Proof. Multiplying both the sides of (2) by $\Delta = 1 = q^{-1}$ results in

$$A_2(q^{-1})\Delta y(k) = B_2(q^{-1})\Delta w(k). \tag{38}$$

From (3), we get

$$\Delta w(k) = (\partial_{\hat{v}}\hat{w})_k|\Delta v(k)|. \tag{39}$$

Then, in terms of (1) and (22), this leads to

$$A_1(q^{-1})v(k) = q^{-d}B_1(q^{-1})\Delta^{-1}\gamma e(k+d)\psi(k). \tag{40}$$

Rearranging (40) yields

$$A_1(q^{-d})\Delta v(k) = q^{-1}B_1(q^{-1})\gamma e(k+d)\psi(k). \tag{41}$$

Then, combining (38), (39) and (41) results in

$$\begin{aligned} &|A_1(q^{-1})|A_2(q^{-1})\Delta y(k) \\ &\quad = B_2(q^{-1})(\partial_{\hat{v}}\hat{w})_k \\ &\qquad \cdot |q^{-d}B_1(q^{-1})\gamma e(k+d)\psi(k)|. \end{aligned} \tag{42}$$

Based on Lemma 2, for the bounded input u, y is also bounded, i.e., for $\eta_{1u} > 0$, $|y(k)| \le \eta_{1u}$. Thus,

$$\begin{aligned} 0 &< |q^{-d}B_1(q^{-1})B_2(q^{-1})(\partial_{\hat{v}}\hat{w})_k\gamma e(k+d)\psi^2(k)| \\ &= |A_1(q^{-1})A_2(q^{-1})\Delta y(k)| \\ &\le \eta_{1u}|\Delta||A_1(q^{-1})A_2(q^{-1})|. \end{aligned} \tag{43}$$

Then, based on Lemma 3, $(\partial_{\hat{v}}\hat{w})_k$ and $\psi(k)$ are all bounded. In this case, taking the limit of (43) results in

$$\begin{aligned} 0 &< \gamma|B_1(q^{-1})B_2(q^{-1})||(\partial_{\hat{v}}\hat{w})_k||\psi^2(k)||e(k+d)|_{q^{-1}\to 1} \\ &\le \lim_{q^{-1}\to 1} \eta_{1u}|\Delta||A_1(q^{-1})|A_2(q^{-1})| \to 0. \end{aligned} \tag{44}$$

Therefore, $e(k+d) \to 0$ as $k \to \infty$. ■

5. Experimental results

The proposed NOC-MEC scheme is validated on an MPS with a PEA as shown in Fig. 4, where a three-dimensional micropositioning stage driven by PEA is illustrated. On each axis, an amplifier with a filtering circuit is used to drive the piezoelectric actuator to produce deformation, which is amplified by the flexure hinge to drive the load. Then, the displacement of the load is measured by the integrated capacitive positioning sensor. In addition, the measured displacement signal is amplified by the conditioning circuit and then sampled by a 12-bit A/D converter and fed to the computer. After that, the digital control signal sent out by the computer is converted into an analogy signal by a 12-bit D/A converter, then amplified by the amplifier with the filtering circuit to drive the piezoelectric actuator. In this paper, the NOC-MEC scheme is only tested on the X-axis of the stage.

To describe the characteristic of the single-axis system, a sandwich model with hysteresis as shown in Fig. 1 is constructed. In this model, L_1 is utilized to describe the characteristic of the amplifier with filtering circuit, and L_2 is employed to depict the flexure hinge with the load driven by the PEA, N is a Duhem submodel used to describe the hysteresis feature of the PEA in the system.

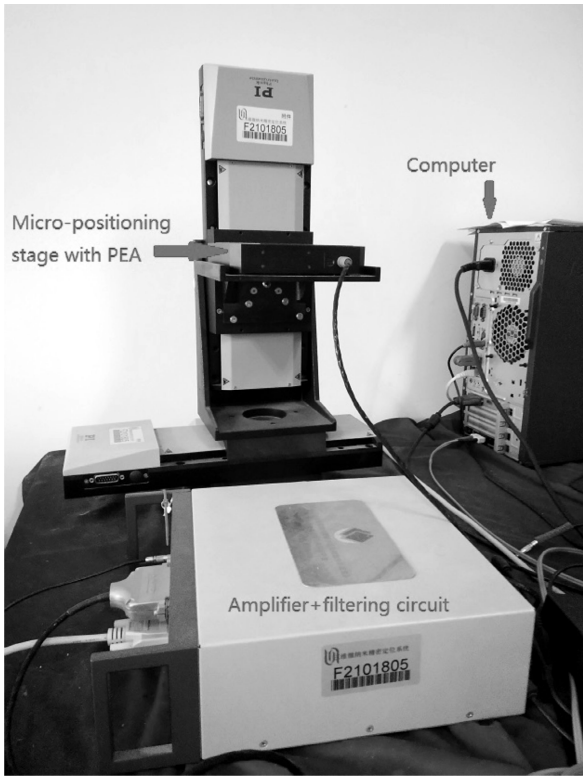

Fig. 4. Micropositioning stage driven by the PEA.

Moreover, u is the input voltage sent to the amplifier with the filtering circuit, v is the actuated voltage output by the amplifier with filtering circuit, w denotes the force of PEA, and y represents the displacement of the flexure hinge with the load.

5.1. Sandwich model with hysteresis. In the case when the sampling period is chosen as $T_s = 0.001$ ms, the step-response of the MPS with the PEA is shown in Fig. 5. It is shown that a time delay exists in the system and the underdamped oscillation occurs due to the influence of hysteresis.

Then, the sandwich model with hysteresis used to describe the characteristics of the MPS with the PEA was obtained by using the recursive identification method of Dong *et al*. (2017). Due to the chosen sampling frequency, the resulting time delay is $d = 5$. Based on the obtained model, the input linear submodel used to describe the characteristic of the amplifier with filtering circuit is

$$L_1 : (1-0.7491q^{-1})\hat{v}(k) = q^{-5}(1+0.7q^{-1})u(k), \quad (45)$$

while the output linear submodel to depict the property of the flexure hinge with load is

$$L_2 : (1 - 1.2q^{-1} + 0.31q^{-2})\hat{y}(k) = (0.05 + 0.005q^{-1})\hat{w}(k), \quad (46)$$

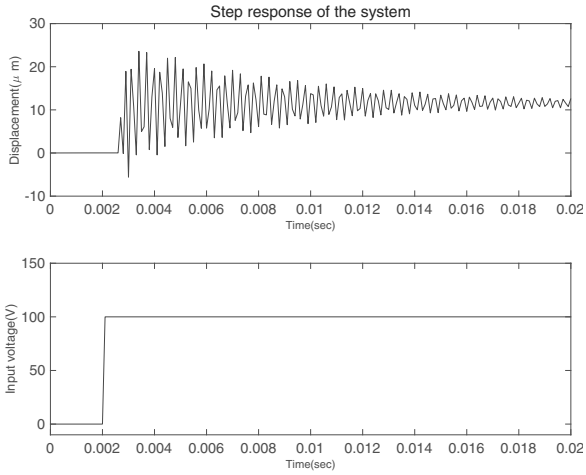

Fig. 5. Step response of the MPS with the PEA.

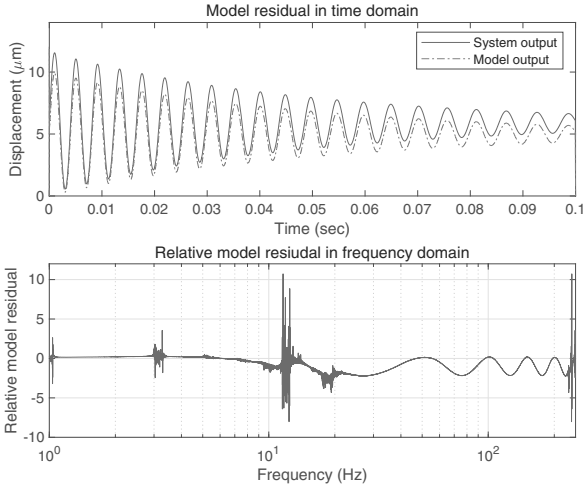

Fig. 6. Model residual in time domain and relative the model residual in frequency domain.

and the hysteresis feature of the piezo-actuator is modeled by

$$\begin{aligned} N : \hat{w}(k) &= \hat{w}(k-1) + 0.024[0.65\,\mathrm{sgn}(\hat{v}(k-1)) + 0.19\hat{v}(k-1) \\ &\quad - \hat{w}(k-1)]|\Delta\hat{v}(k)| + 0.14\Delta\hat{v}(k). \end{aligned} \quad (47)$$

When the sinusoidal input with attenuated amplitude and frequency, i.e.,

$$r(kT_s) = 5e^{-20kT_s}\sin(500\pi e^{-2kT_s}kT_s) + 5,$$

is fed to the piezo-actuated micropositioning stage and the above-stated model, the corresponding response difference between the piezo-MPS and the obtained model is illustrated in Fig. 6. It can be seen that the system has obvious model residuals. In addition, the amplitude frequency curve of the relative model residual is also

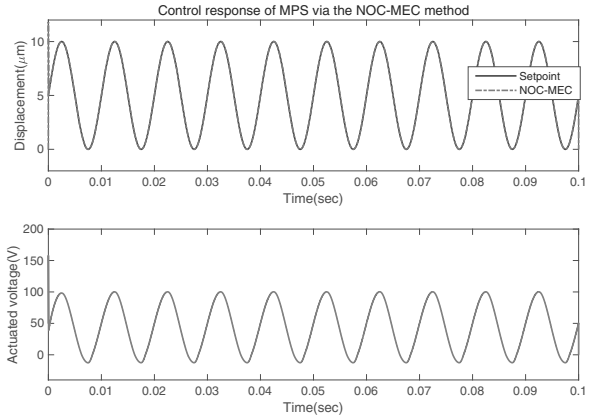

Fig. 7. Control response of the MPS via the NOC-MEC method.

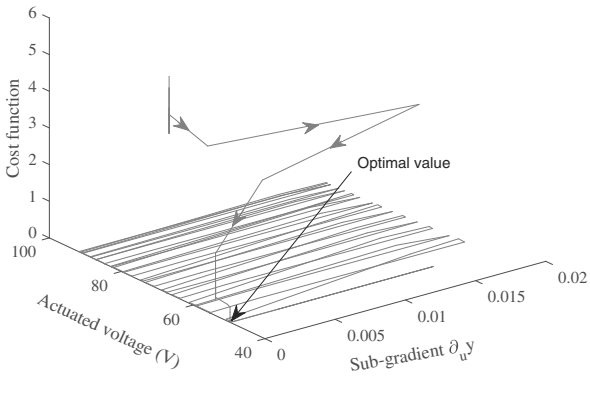

Fig. 8. Optimized search process.

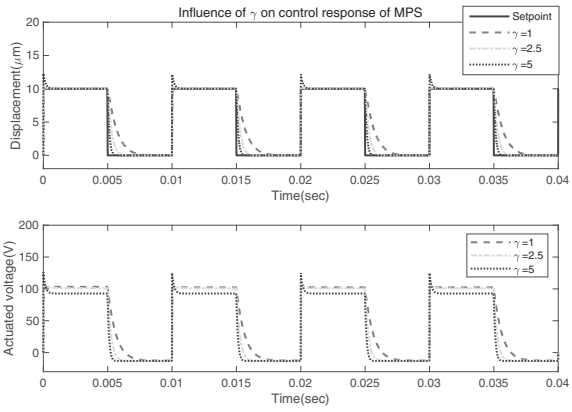

Fig. 9. Influence of γ on the control response of the MPS.

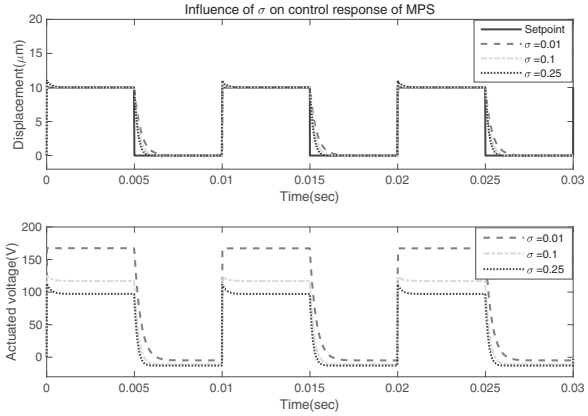

Fig. 10. Influence of σ on the control response of the MPS.

shown in Fig. 6. It can be seen that the resonance peaks occur at about 10.2 Hz and at a higher frequency of about 250 Hz. To deal with the displacement control of the positioning system with model uncertainty, the nonsmooth optimization control law represented by (21) and (22) is applied to the control of the piezo-positioning stage.

5.2. Reference trajectory tracking. To test the tracking performance of the NOC-MEC method, the reference trajectory of the MPS is a sinusoidal signal, i.e., $r(k) = 5\sin(2\pi fk) + 5$, $f = 100$ Hz. The control parameters are selected as $\beta = 0.5$, $\gamma = 36$ and $\sigma = 0.23$, respectively. The corresponding control response is shown in Fig. 7. It is seen that the proposed control scheme has achieved satisfactory control performance.

Moreover, Fig. 8 demonstrates the search process of the control system within one sampling period via iteration. It is seen that the cost function is not smooth due to the existence of nonsmooth hysteresis. Using the proposed search, an optimal value of the system can be reached.

It is known that the optimization stepsize γ in the NOC-MEC control scheme has significant influence on the control performance. By fixing $\sigma = 0.25$ and choosing different values of γ, the comparison of the corresponding control responses is shown in Fig. 9. From the figure it is clear that the sluggish response is obtained when the value of γ is chosen to be 1. However, when $\gamma = 2.5$, the resulting control response is fast and stable. On the other hand, the aggressive response with overshoot is produced as the value of γ is chosen as 5. Therefore, it can be concluded that smaller values of γ will lead to slow control responses and larger values of γ will speed up the responses, but may also lead to overshoot and oscillation of the control response.

For evaluating the effect of the compensation factor shown in (8) and (9) on NOC-MEC control performance, let σ be 0.01, 0.1 and 0.25, respectively, with the fixed $\beta = 0.5$ and $\gamma = 3.5$. Figure 10 illustrates the responses of the control scheme with the NOC-MEC when σ is with the chosen values. When the value of σ is 0.01, the system exhibits a sluggish response. On the other hand, when σ equals 0.25, it results in a more aggressive and faster response than the cases of choosing smaller values of σ. In addition, when σ is 0.25, the overshoot occurs in

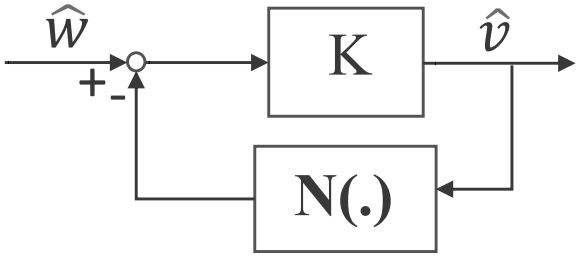

Fig. 11. Structure diagram of the pseudoinverse hysteresis submodel.

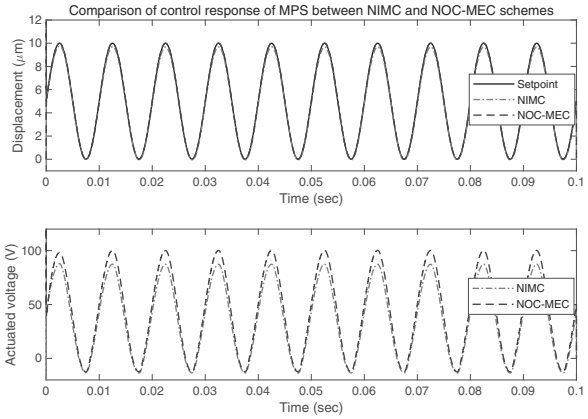

Fig. 12. Comparison of the positioning control response between the NIMC and NOC-MEC methods (sinusoidal setpoint).

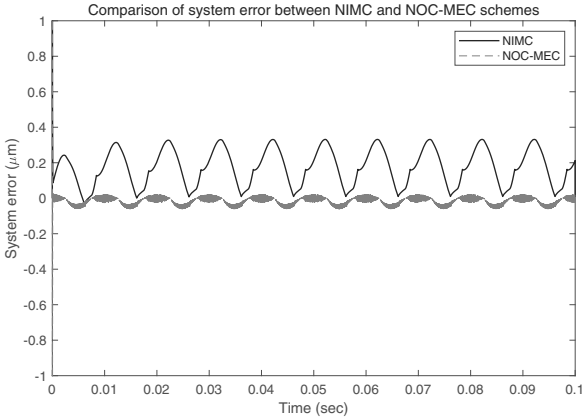

Fig. 13. Comparison of the system error between the NIMC and NOC-MEC methods.

the system response. The results show that the overshoot increases rapidly as the value of σ increases.

5.3. Comparing NOC-MEC with nonlinear NIMC method. In order to evaluate the robustness of the proposed NOC-MEC strategy, it is compared with the nonlinear internal model control (NIMC) method, which is a well-known robust control strategy. To design the nonlinear internal model controller, based on (45) and (46), the corresponding inverse submodels of L_1 and L_2 are described by $L_1^{-1}(q^{-1}) = u(k)/\hat{v}(k) \approx (1 - 0.7491q^{-1})/(1 + 0.7q^{-1})$ and $L_2^{-1}(q^{-1}) = \hat{w}(k)/\hat{y}(k) \approx (1-1.2q^{-1}+0.31q^{-2})/(0.05+0.005q^{-1})$, respectively. In addition, the inverse hysteresis submodel is approximated based on the pseudoinverse structure (Dong *et al.*, 2020) as shown in Fig. 11, where $\hat{v}(k) = K\hat{w}(k)/(1 + N(\cdot)K)$. When gain K is chosen to let $|KN(.)| \gg 1$, this leads to $\hat{v}(k) = N^{-1}(\cdot)\hat{w}(k)$ approximately.

Thus, the corresponding NIMC strategy is designed as

$$u(k) = L_2^{-1}(q^{-1})N^{-1}(\cdot)L_1^{-1}(q^{-1})F(q^{-1})e_I(k), \quad (48)$$

where $F(q^{-1})$ is a robust filter and $e_I(k) = r(k) - y(k) + \hat{y}(k)$ is the system error. In the experiment, the parameters of the NOC-MEC method are chosen as $\beta = 0.5$, $\gamma = 36$ and $\sigma = 0.23$. On the other hand, based on the relative model residual shown in Fig. 6, the robust filter of the NIMC scheme is chosen as $F(q^{-1}) = 0.0128/(1 - 0.995q^{-1})$. Moreover, the setpoint of the micro-positioning stage is $r(k) = 5\sin(200\pi k) + 5$. The corresponding comparisons of the controlled system response and system error between the NOC-MEC and NIMC methods are shown in Figs. 12 and 13, respectively.

Moreover, when the setpoint is a sawtooth wave sequence with the frequency $f = 50$ Hz and amplitude varying from 0 to 10 μm, the parameters of the NOC-MEC strategy are $\beta = 0.5$, $\gamma = 3.5$ and $\sigma = 0.23$. Then, the robust filter of the NIMC scheme is $F(q^{-1}) = 0.0384/(1 - 0.985q^{-1})$. Figures 14 and 15 respectively show the comparisons of control responses between the NIMC and NOC-MEC methods and the corresponding comparison of the controlled system errors between the two methods.

Through those comparisons, it can be seen that the proposed NOC-MEC method achieves a more accurate tracking response than the NIMC method. The results show that the NOC-MEC method has a good ability to compensate the influence of the model uncertainty. This is because the integrated model error compensator in the NOC-MEC method compensates the influence of the model error, which can improve the dynamic performance of the system and yield faster and more accurate tracking control performance. In addition, it can be seen that although the NIMC method can also deal with model uncertainty, its robust stability design of the controller leads to a more conservative control effect and slower tracking performance.

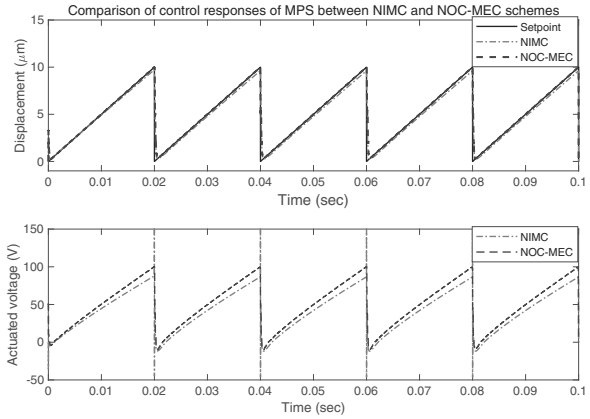

Fig. 14. Comparison of the control responses between the NIMC and NOC-MEC methods when the setpoint is a sawtooth wave.

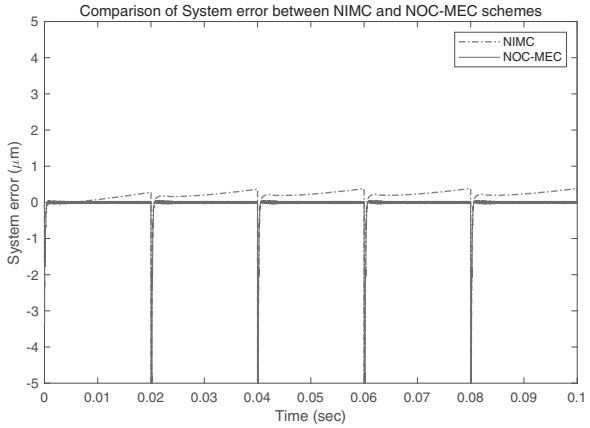

Fig. 15. Comparison of the controlled system errors between the NIMC and NOC-MEC methods when the setpoint is sawtooth wave.

6. Conclusion

In this paper, a sandwich model with hysteresis is used to describe the micropositioning stage with piezo- actuators. Then the online nonsmooth optimization control method for the sandwich systems with hysteresis is proposed. Due to the existence of nonsmooth hysteresis, the gradients of the cost function of the nonsmooth sandwich system with respect to the control input do not exist at nonsmooth points. Thus, the subgradient of the nonsmooth cost function with respect to the control input is applied. To avoid the complicated calculation of online search for an optimal value of the subgradient which is, in fact, a close interval at nonsmooth point, the estimation of the subgradient with smooth interpolation is proposed.

To tackle the influence of model uncertainty, a model error compensator is integrated in the control strategy. Thus, the robust stability of the resulting NOC-MEC strategy can be enhanced and the tracking performance of the system can be improved. Moreover, the stability of the control system is analyzed by Lyapunov's method. Compared with the NIMC strategy, the verification results of the proposed NOC-MEC method on the MPS with the PEA system show that the proposed scheme has achieved much more satisfactory performance.

Because of the complexity of sandwich models, it is very difficult to identify a specific sandwich model. In the next step, it is very meaningful to consider how to realize the optimal control of the model-free sandwich system.

Acknowledgment

This work was supported by the National Natural Science Foundation of China under the grants 62171285 and 61971120.

References

Chen, X. (2012). Smoothing methods for nonsmooth, nonconvex minimization, *Mathematical Programming* **134**(1): 71–79.

Clarke, D.W., Mohtadi, C. and Tuffs, P.S. (1987). Generalized predictive control. Part II: Extensions and interpretations, *Automatica* **23**(2): 149–160.

Clarke, F., Ledyaev, Y., Stern, R. and Wolenski, P. (1998). *Nonsmooth Analysis and Control Theory*, Springer, New York.

Corradini, M., Orlando, G. and Parlangeli, G. (2005). Robust control of nonlinear uncertain systems with sandwiched backlash, *Proceedings of the 44th IEEE Conference on Decision and Control, Seville, Spain*, pp. 8112–8117.

Dong, R., Tan, Q. and Tan, Y. (2008). A nonsmooth nonlinear programming based predictive control for mechanical servo systems with backlash-like hysteresis, *Asian Journal of Control* **20**(4): 1519–1532.

Dong, R., Tan, Y. and He, D. (2013). A non-smooth IMC method for mechanical systems with backlash, *Journal of Control Theory Applications* **11**(4): 600–607.

Dong, R., Tan, Y. and Tan, Q. (2020). Mirror angle tuning of electromagnetic micro-mirrors with oscillation compensation, *IEEE Transactions on Systems, Man and Cybernetics: Systems* **50**(8): 2969–2977.

Dong, R., Tan, Y. and Xie, Y. (2016). Identification of micropositioning stage with piezoelectric actuators, *Mechanical Systems and Signal Processing* **75**: 618–630.

Dong, R., Tan, Y., Xie, Y. and Janschek, K. (2017). Recursive identification of micropositioning stage based on sandwich model with hysteresis, *IEEE Transactions on Control Systems Technology* **25**(1): 317–325.

Harnischmacher, G. and Marquardt, W. (2007). Nonlinear model predictive control of multivariable processes using block-structured models, *Control Engineering Practice* **15**(10): 1328–1256.

Janaideh, M., Su, C. and Rakheja, S. (2008). Development of the rate-dependent Prandtl–Ishlinskii model for smart actuators, *Smart Materials and Structures* **17**(3): 035026.

Li, Y., Liu, Y. and Tong, S. (2022). Observer-based neuro-adaptive optimized control for strict-feedback nonlinear systems with state constraints, *IEEE Transactions on Neural Networks and Learning Systems* **33**(7): 3131–3145.

Luo, N., Tan, Y. and Dong, R. (2015). Observability and controllability analysis for sandwich systems with backlash, *International Journal of Applied Mathematics and Computer Science* **25**(4): 803–814, DOI: 10.1515/amcs-2015-0057.

Manni, A., Parlangeli, G. and Corradini, M. (2008). Robust stabilization of nonlinear sandwich plants containing generalized hysteresis nonlinearities, *Proceedings of the 17th World Congress of the International Federation of Automatic Control, Seoul, Korea*, pp. 14409–14414.

Oh, J. and Bernstein, D. (2005). Semilinear Duhem model for rate-independent and rate-dependent hysteresis, *IEEE Transactions on Automatic Control* **50**(5): 631–645.

Oliveri, A., Maselli, M., Lodi, M., Storace, M. and Cianchetti, M. (2019). Model based compensation of rate-dependent hysteresis in a piezoresistive strain sensor, *IEEE Transactions on Industrial Electronics* **66**(10): 8205–8213.

Tao, G., Ma, X. and Ling, Y. (2001). Optimal and nonlinear decoupling control of system with sandwiched backlash, *Automatica* **37**(2): 165–176.

Taware, A., Tao, G. and Teolis, C. (2002). Design and analysis of a hybrid control scheme for sandwich non-smooth nonlinear systems, *IEEE Transactions on Automatic Control* **47**(1): 145–150.

Tong, S., Sun, K. and Sui, S. (2018). Observer-based adaptive fuzzy decentralized optimal control design for strict feedback nonlinear large-scale systems, *IEEE Transactions on Fuzzy Systems* **26**(2): 569–584.

Xie, Y., Tan, Y. and Dong, R. (2013). Nonlinear modeling and decoupling control of XY micropositioning stages with piezoelectric actuators, *IEEE/ASME Transactions on Mechatronics* **18**(3): 821–832.

Xue, Y., Meng, D., Yin, S., Han, W., Yan, X., Shu, Z. and Diao, L. (2019). Vector-based model predictive hysteresis current control for asynchronous motor, *IEEE Transactions on Industrial Electronics* **66**(11): 8703–8712.

Yu, D., Long, J., Chen, C.L.P. and Wang, Z. (2022). Adaptive swarm control within saturated input based on nonlinear coupling degree, *IEEE Transactions on Systems, Man, and Cybernetics: Systems* **52**(8): 4900–4911.

Zhang, Z., Yang, Z., Liu, S., Chen, S. and Zhang, X. (2022). A multi-model based adaptive reconfiguration control scheme for an electro-hydraulic position servo system, *International Journal of Applied Mathematics and Computer Science* **32**(2): 185–196, DOI: 10.34768/amcs-2022-0014.

Zhao, X. and Tan, Y. (2006). Neural adaptive control of dynamic sandwich systems with hysteresis, *Proceedings of 2006 IEEE International Symposium on Intelligent Control, Munich, Germany*, pp. 82–87.

Sen Yang obtained his MS degree in mathematics in 2008 from the Xi'an University of Architecture and Technology, China. From 2007 to 2016, he was a lecturer at the Henan University of Science and Technology, Luoyang, China. At present, he is a PhD candidate at the College of Mathematics and Science, Shanghai Normal University, China. His research interests are in optimization, control and state estimation of nonlinear dynamic systems.

Yonghong Tan received his PhD degree in electrical engineering in 1996 from the University of Ghent, Belgium. He was a postdoctoral fellow at Simon Fraser University, Vancouver, BC, Canada, from 1996 to 1998. He is currently a professor in the College of Information, Mechanical and Electrical Engineering, Shanghai Normal University, China. Doctor Tan had held professorships at the Guilin University of Electronic Technology and the University of Electronic Science and Technology of China. His research interests are in modeling and control of nonlinear systems, mechatronics, signal processing and fault diagnosis of micro/nano systems.

Ruili Dong received her PhD degree from Shanghai Jiaotong University, China, in 2009. She was a visiting scholar with the University of Illinois at Chicago, USA, from 2012 to 2013. From 2014 to 2016, she was a post-doctoral fellow at the Dresden University of Technology, Germany. She was a research fellow at the University of Windsor, ON, Canada, from 2016 to 2017. Presently, she is a professor at the College of Information Science and Technology, Donghua University, Shanghai, China. Her research interests are in identification and control of nonlinear systems and micro/nano mechatronic systems.

Qingyuan Tan received his BEng degree in instrumentation and control science from Shanghai Jiao Tong University, China, in 2010, his MS degree in mechanical engineering from the University of Toronto, ON, Canada, in 2013, and his PhD degree in electrical engineering from the University of Windsor, ON, Canada, in 2018. His research interests are in modeling and control of mechatronic systems, powertrain control systems, and intelligent vehicle control.

Appendix A

Proof of Lemma 2

For a given $\eta_u > 0$, we have $|u(k)| \leq \eta_u$. Based on Assumption 1, $|L_1(\cdot)| < +\infty$ and $|L_2(\cdot)| < +\infty$, which leads to

$$|v(k)| \leq |L_1(\cdot)|\eta_u. \tag{A1}$$

Then, according to Lemma 1, defining $\mu \triangleq \alpha|\Delta v(k)| - 1$ results in $0 < \mu < 1$. Obviously, $1/|1 + \mu q^{-1}|$ is bounded, i.e., for a given $\eta_\mu > 0$, we

have $1/|1+\mu q^{-1}| \le \eta_\mu$. Rearranging (3) yields

$$\begin{aligned}|w(k)| &= \\ &\frac{|\alpha||[f_0\,\mathrm{sgn}(v(k-1))+f_1 v(k-1)]|\Delta v(k)|+g_0\Delta v(k)|}{|1+(\alpha\Delta v(k)-1)q^{-1}|} \\ &\le \frac{2(|f_0\,\mathrm{sgn}(v(k-1))+f_1 v(k-1)|+|g_0|/|\alpha|)}{|1+(\alpha\Delta v(k)-1)q^{-1}|} \\ &\le 2\eta_\mu(|f_0|+|f_1||L_1(\cdot)|\eta_\mu+\frac{|g_0|}{|\alpha|}).\end{aligned} \tag{A2}$$

Define

$$\eta_w = 2\eta_\mu\left(|f_0|+|f_1||L_1(\cdot)|\eta_\mu+\frac{|g_0|}{|\alpha|}\right). \tag{A3}$$

Thus, $|w(k)| \le \eta_w$, i.e., $w(k)$ is also bounded. Based on Assumption 1, it can be seen that

$$|y(k)| \le |L_2(\cdot)||w(k)|. \tag{A4}$$

Since $|L_2(\cdot)| < +\infty$ and $|w(k)| \le \eta_w$, $y(k)$ is also bounded.

Appendix B
Proof of Lemma 3

In terms of Assumption 1, (5) and (A1), $\hat{v}(k+1|k)$ is bounded for the bounded input $u(k)$. From (6), (A2), (A3) and Lemma 1, $\hat{w}(k)$ is also bounded.

Hence, F_k^+ described by (18) and F_k^- described by (19) are all bounded; in other words, there exists a positive constant η_v, which leads to

$$\begin{aligned}|F_k^+| &= |g_0+\alpha[f_0\,\mathrm{sgn}(\hat{v}(k))+f_1\hat{v}(k)-\hat{w}(k)]| \\ &\le |g_0|+|\alpha|(|f_0|+|f_1||L_1(\cdot)||\eta_u|+|\eta_w|).\end{aligned} \tag{B1}$$

Defining $\eta_1 = |g_0|+|\alpha|(|f_0|+|f_1||L_1(\cdot)||\eta_u|+|\eta_w|)$ yields

$$|F_k^+| \le \eta_1. \tag{B2}$$

Similarly, we also get

$$|F_k^-| \le \eta_1. \tag{B3}$$

Then

$$\begin{aligned}&|\beta F_k^+ + (1-\beta)F_k^-| \\ &\qquad \le \beta|F_k^+| + (1-\beta)|F_k^-| \le \eta_1.\end{aligned} \tag{B4}$$

Based on (20) and (B2)–(B4), this leads to

$$|(\partial_{\hat{v}}\hat{w})_k| \le \eta_1. \tag{B5}$$

Since $|\partial_{u(k-1)}\phi(\varepsilon(k))| \le \eta_0$, defining $\eta_v = |r_1 b_{20}|\eta_1+\eta_0$ leads to

$$\begin{aligned}|\psi(k)| &= |r_1 b_{20}(\partial_{\hat{v}}\hat{w})_k + \partial_{u(k-1)}\phi(\varepsilon(k))| \\ &\le |r_1 b_{20}||(\partial_{\hat{v}}\hat{w})_k| + |\partial_{u(k-1)}\phi(\varepsilon(k))| \\ &\le |r_1 b_{20}|\eta_1+\eta_0 = \eta_v.\end{aligned} \tag{B6}$$

Received: 8 December 2022
Revised: 9 February 2023
Accepted: 14 February 2023